A&A 423, 1051–1061 (2004)
DOI: 10.1051/0004-6361:20035898


Astronomy & Astrophysics

# Seismic extraction of the convective extent in solar-like stars

## The observational point of view⋆

J. Ballot, S. Turck-Chièze, and R. A. García

Service d'Astrophysique, CEA/DSM/DAPNIA, CE Saclay, 91191 Gif-sur-Yvette Cedex, France
e-mail: [jballot;cturck;rgarcia]@cea.fr

Received 18 December 2003 / Accepted 29 April 2004

**Abstract.** Convection is the first manifestation of macroscopic motions in stars. In the next decade, the extent of the external convective zone of solar-like stars will have to be derived from the eigenfrequencies of their low-degree ($\ell = 0, 1$ and 2) acoustic modes. In this paper, we compare different tracers of the base of the convective zone (BCZ) and show that the second difference $\delta_2\nu$ stays simple and well suited for analyzing real data. We suggest the use of $\tilde{t}_{\rm BCZ} = (2\langle\Delta\nu\rangle)^{-1} - \tilde{\tau}_{\rm BCZ}$ as a quasi-non-biased indicator of the BCZ acoustic *radius*. The method is first checked on a long-time solar observation with GOLF, then on shorter real observations by VIRGO and 10 000 simulated observations of solar-like stars. We present results for different observational duration and stellar masses. The intrinsic error due to the method on the convective extent is smaller than 1.5% (in units of stellar acoustic radius) for stars with masses between 0.9 and 1.3 $M_\odot$. The limited observational interval adds a supplementary uncertainty of about 1.6% for a 150-day long simulated observation. In this study, we have also analyzed the effects of stochastic excitation and of non-continuous runs of shorter lengths. We discuss how to take into account the variations in activity.

**Key words.** convection – stars: oscillations – stars: interiors – Sun: helioseismology – methods: data analysis

## 1. Introduction

Thanks to the observations provided by ground-based networks or by the SoHO[1] spacecraft, helioseismology has allowed the astrophysicists to considerably improve the information on the solar interior, and most of the physical processes that govern it have been studied independently. For example, the helium surface abundance has been determined (Vorontsov et al. 1991) and the microscopic diffusion (e.g. Michaud & Proffitt 1993) has been clearly quantified and introduced in stellar modelling. Dynamical effects, especially in the tachocline (Spiegel & Zahn 1992; Brun et al. 1999), have been taken into account and a problem as old as the solar neutrino puzzle has recently been solved without ambiguity (Turck-Chièze et al. 2001; Couvidat et al. 2003). The challenge of future asteroseismic missions like CoRoT (Baglin & The CoRoT Team 1998) or Eddington (Favata et al. 2003) is to continue to improve our knowledge of stellar interiors, especially of the dynamical processes occurring there. The main dynamical phenomenon occurring of the stars is convection. A first step consists of determining the extent of the convective region for solar-like stars. The objective is to go beyond the two classic methods treating convection in stellar evolution: one is based on the mixing length parameter scaled to the unique solar case and the second is based on the treatment of the overshooting, which has shown its limitations in the lithium burning problem in young solar-like stars (e.g. Ventura et al. 1998; Piau & Turck-Chièze 2002).

The position of the BCZ in the Sun has been accurately known for more than ten years (e.g. Christensen-Dalsgaard et al. 1991) thanks to the extraction of the sound speed by inversion techniques. In this case, the very good accuracy is due to the use of high- and intermediate-degree modes, but for other stars we shall not be able to observe these modes: only low-degree modes will be determined in the near future. Specific inversion tools are required to exploit them (Marchenkov et al. 2000; Roxburgh & Vorontsov 2003). However the depth of the convective region can be directly derived from the frequencies. It is now well known (e.g. Gough 1990) that a steep variation of the sound speed – like at the BCZ – leads to oscillations in observable seismic parameters. These oscillations can directly be found in the frequencies ($\nu = \omega/2\pi$) (Monteiro et al. 1994, 2000), in the large separation ($\Delta\nu_{\ell,n} = \nu_{\ell,n+1} - \nu_{\ell,n} \equiv \delta_1\nu_{\ell,n}$), in the second difference ($\delta_2\nu_{\ell,n} = \nu_{\ell,n-1} - 2\nu_{\ell,n} + \nu_{\ell,n+1}$), in the higher order differences $\delta_k\nu$ (e.g. Basu 1997; Mazumdar & Antia 2001) or in other variables like the phase-shift derivative $\beta$ (Lopes & Turck-Chièze 1994; Roxburgh & Vorontsov 1994, 1996, 2001; Lopes et al. 1997).

⋆ Appendix B is only available in electronic form at http://www.edpsciences.org

[1] Solar and Heliospheric Observatory.

## 2. Extraction of the BCZ

This modulation in the variables can be written as the following additive correction:

$$\delta\mathrm{Var} = A_{\mathrm{Var}}(\omega)\cos[2(\tilde{\tau}_{\mathrm{BCZ}}\omega + \phi_0)] \quad (1)$$

where Var is the considered variable: $\nu$, $\Delta\nu$, $\delta_2\nu$, ... , $\delta_k\nu$ or $\beta$ and where $\tilde{\tau}_{\mathrm{BCZ}} = \tau_{\mathrm{BCZ}} + a_\phi$. $a_\phi$ and $\phi_0$ are constants. $\tau_{\mathrm{BCZ}} = T - t_{\mathrm{BCZ}}$ is the BCZ acoustic depth, $t_{\mathrm{BCZ}}$ the acoustic radius of the BCZ and $T$ the acoustic radius of the star:

$$t_{\mathrm{BCZ}} = t(r_{\mathrm{BCZ}}) = \int_0^{r_{\mathrm{BCZ}}} \frac{\mathrm{d}r}{c(r)} \quad (2)$$

$$T = t(R_*) \quad (3)$$

$r_{\mathrm{BCZ}}$ is the position of the BCZ, $R_*$ is the stellar photospheric radius and $c$ is the sound speed.

The oscillation amplitude $A_\nu(\omega)$ depends on the physical properties of the radiation/convection transition, especially on the discontinuity of the sound-speed second derivative (e.g. Roxburgh & Vorontsov 2001). The study of the shape of this amplitude can provide structural information like overshoot characteristics (e.g. Monteiro et al. 2000), but we do not discuss this aspect here. From $A_\nu(\omega)$, it is straight forward to deduce $A_{\delta_k\nu}(\omega)$:

$$\begin{aligned} A_{\delta_k\nu}(\omega) &\simeq (2\sin(2\pi\tilde{\tau}_{\mathrm{BCZ}}\langle\Delta\nu\rangle))^k A_\nu(\omega) \\ &\simeq \left(2\sin\left(\pi\frac{t_{\mathrm{BCZ}}}{T}\right)\right)^k A_\nu(\omega) \end{aligned} \quad (4)$$

with $\langle\Delta\nu\rangle$ the mean large separation. We have also assumed that $T \simeq (2\langle\Delta\nu\rangle)^{-1}$ (e.g. Tassoul 1980).

### 2.1. The choice of the variable

The amplitude of the searched signature increases with the difference order if $\sin(\pi\frac{t_{\mathrm{BCZ}}}{T}) > 0.5$ (cf. Eq. (4)) which is generally the case for solar-like stars. However the noise increases too. If $\sigma_\nu$ is the typical noise of the frequencies, the noise for the $k^{\mathrm{th}}$-difference is $\sigma^2_{\delta_k\nu} = \sum_{p=0}^{k}\binom{k}{p}^2\sigma^2_\nu$. The signal-to-noise ratios (SNR) $A_{\delta_k\nu}/\sigma_{\delta_k\nu}$ are plotted in Fig. 1 for several differences. As $t_{\mathrm{BCZ}}/T$ is mainly contained between 0.35 and 0.60 for solar-like stars (cf. Table 1), the SNR is increased by taking the differences. This removes the smooth and slowly-variable components due to surface effects. Therefore the signal appears more clearly.

Nevertheless, as more frequencies are used to compute a greater-order difference, fewer points are available with the same frequency set. Furthermore the error propagation is enhanced: one poorly determined frequency corrupts two points of $\Delta\nu$, three of $\delta_2\nu$, ..., seven of $\delta_6\nu$...

Finally a compromise must be made between these two aspects. $\delta_2\nu$ seems to be a good choice, confirmed by the simulations (cf. Sect. 3.4).

### 2.2. The second difference $\delta_2\nu$

The second difference is mainly composed of two oscillations: the first component – larger and slower – is due to the He II ionization region; the second one – smaller and faster – is the signature of the BCZ. Figure 2 illustrates this information using the data obtained with the GOLF[2] instrument aboard the SoHO spacecraft after 6 years of observation. The very good accuracy obtained on the low-degree mode frequencies allows us to directly see these two oscillations in the $\delta_2\nu$ variable. There are two ways to extract and to quantify these oscillations.

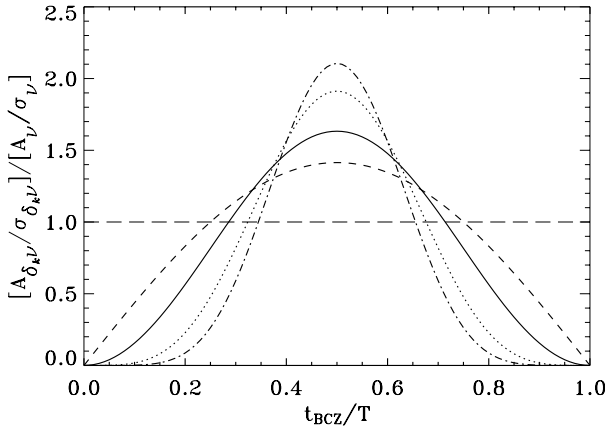


**Fig. 1.** Signal-to-noise ratio ($A_{\delta_k\nu}/\sigma_{\delta_k\nu}$) of the signature of the BCZ in different variables: $\Delta\nu$ (dashed line), $\delta_2\nu$ (solid line), $\delta_4\nu$ (dotted line) and $\delta_6\nu$ (dots and dashes), normalized by the SNR ($A_\nu/\sigma_\nu$) directly observed in the mode frequencies. This relative SNR is plotted as a function of the BCZ acoustic radius ($t_{\mathrm{BCZ}}$) normalized to the stellar acoustic radius ($T$).

Firstly, the variable can be fit with an appropriate expression (e.g. Basu 1997; Mazumdar & Antia 2001) like

$$\begin{aligned} \delta_2\nu = &\left(a_0 + a_1\omega + \frac{a_2}{\omega}\right) \\ &+ \left(b_0 + \frac{b_1}{\omega} + \frac{b_2}{\omega^2}\right)\sin(2\omega\tilde{\tau}_{\mathrm{He}} + \phi_{\mathrm{He}}) \\ &+ \left(c_0 + \frac{c_1}{\omega} + \frac{c_2}{\omega^2}\right)\sin(2\omega\tilde{\tau}_{\mathrm{BCZ}} + \phi_{\mathrm{BCZ}}) \end{aligned} \quad (5)$$

where $a_i$, $b_i$, $c_i$, $\tilde{\tau}_{\mathrm{He}}$, $\phi_{\mathrm{He}}$, $\tilde{\tau}_{\mathrm{BCZ}}$ and $\phi_{\mathrm{BCZ}}$ are the parameters to fit by a non-linear least-squares method. The results of this technique are very accurate, but the method is not very robust because of the non-linearity of the expression. What we mean by *robustness* is the capability of a method or an algorithm to converge to the *correct* solution. A method is robust if it is not very sensitive to the initial conditions and if the solution does not need to be known a priori. This aspect is very important if we want to develop more automatic techniques.

Secondly, a spectral analysis can be applied to extract $2\tilde{\tau}_{\mathrm{BCZ}}$ after removing a smooth component which takes into account the large oscillation. The choice of the smooth component can be discussed. The first idea is to use a polynomial expression, but such an expression has difficulty in describing the global behaviour of $\delta_2\nu$. We could use a more complex (non-linear) function, but we would be confronted with the robustness problem. The best results are obtained with a smoothing by a basic convolution with a box function. The width of the box used is typically $2\Delta\nu$. Thus when the $\ell = 0, 1$ and 2 modes are considered, this interval corresponds

[2] Global Oscillation at Low Frequency.

**Table 1.** The acoustic radius of the star ($T$) and of the BCZ ($t_{\rm BCZ}$) are given for different stellar models (see Sect. 3.1 for more details) as well as their ratio $t_{\rm BCZ}/T$. For each model, one gives the results of BCZ extraction, from a limited frequency set ($\ell$ = 0–2 and $n$ = 14–26), with two techniques: (1) the spectral analysis of $\delta_2\nu$; (2) the fit of Eq. (5) (cf. Sect. 3.2). For each techniques one gives the extracted BCZ acoustic radius ($\tilde{t}_{\rm BCZ}$) with its uncertainty ($\sigma_{\tilde{t}}/T$) and the relative error made ($\tilde{t}_{\rm BCZ} - t_{\rm BCZ}$)/$T$. For the first method, the error bar is deduced from the HWHM ($\sigma_{\tilde{t}} \equiv \sigma_{\tilde{t}}^{\rm sp}$); for the second one, the error is provided by the method of least-squares fit ($\sigma_{\tilde{t}} \equiv \sigma_{\tilde{t}}^{\rm fit}$).

| | Input model | | | From frequencies | | | |
|---|---|---|---|---|---|---|---|
| Star | $T$ (s) | $t_{\rm BCZ}$ (s) | $t_{\rm BCZ}/T$ | $\tilde{t}_{\rm BCZ}$ (s) | $\sigma_{\tilde{t}}/T$ | $\frac{\tilde{t}_{\rm BCZ}-t_{\rm BCZ}}{T}$ | |
| Sun (SEISMIC$_1$) | 3520 | 1420 | 0.40 | 1400 | 4.50% | −0.55% | (1) |
| | | | | *1404* | *1.67%* | *−0.45%* | *(2)* |
| $\alpha$ Cen A | 4507 | 2107 | 0.47 | 2045 | 3.93% | −1.36% | |
| | | | | *2063* | *1.55%* | *−0.97%* | |
| M1.30 @ 20 Myr | 4457 | 2432 | 0.55 | 2403 | 5.28% | −0.63% | |
| | | | | *2402* | *1.99%* | *−0.67%* | |
| — @ 100 Myr | 4353 | 2578 | 0.59 | 2520 | 4.43% | −1.33% | |
| | | | | *2518* | *1.52%* | *−1.36%* | |
| — @ 2.4 Gyr | 5735 | 3195 | 0.56 | 3242 | 4.30% | 0.82% | |
| | | | | *3198* | *0.78%* | *0.06%* | |
| — @ 3.15 Gyr | 6413 | 3213 | 0.50 | 3091 | 5.45% | −1.89% | |
| | | | | *3183* | *0.60%* | *−0.46%* | |
| M0.90 @ 50 Myr | 2690 | 1070 | 0.40 | 1037 | 4.63% | −1.22% | |
| | | | | *1045* | *1.16%* | *−0.91%* | |
| — @ 5 Gyr | 2979 | 1151 | 0.39 | 1122 | 4.58% | −0.96% | |
| | | | | *1130* | *1.24%* | *−0.69%* | |
| — @ 10 Gyr | 3490 | 1285 | 0.37 | 1270 | 4.44% | −0.40% | |
| | | | | *1262* | *1.32%* | *−0.65%* | |
| — @ 15 Gyr | 4774 | 1514 | 0.32 | 1537 | 4.67% | 0.49% | |
| | | | | *1533* | *2.04%* | *0.40%* | |

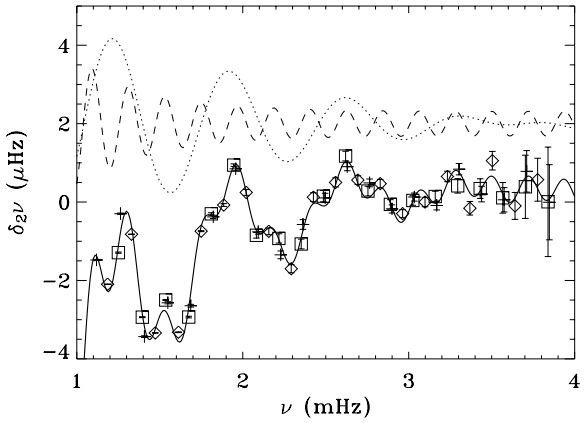


**Fig. 2.** The second difference $\delta_2\nu$ observed in the Sun with GOLF after 6-year observations. Symbols: +: $\ell$ = 0, ◇: $\ell$ = 1 and □: $\ell$ = 2. The solid curve is a least-squares fit of the data with Eq. (5). Both oscillating components are plotted: the dotted line shows the effect of the He II ionization and the dashed one the oscillation due to the BCZ.

to seven points. As the points are not equally spaced, we cannot directly use the classically implemented functions which are designed for regular grids. Thus we have coded a new function, based on the standard mathematical formula, but adapted to non-regular grids. The spectral analysis we have applied to the residue to extract $2\tilde{\tau}_{\rm BCZ}$ is a Fourier-type method based on sine-wave fits. This method is less accurate than the previous one but more robust. This is why this technique will be preferentially used hereafter.

$\tilde{\tau}_{\rm BCZ}$ is measured with these two techniques, but this estimation of $\tau_{\rm BCZ}$ is biased by $a_\phi$, which is not determined. However we can write that $a_\phi \simeq -\pi\frac{{\rm d}\alpha}{{\rm d}\omega}$ ($\simeq$200 s for the Sun, e.g. Christensen-Dalsgaard et al. 1995) where $\alpha$ is the surface phase shift (e.g. Vorontsov et al. 1991).

To remove this bias, we computed an estimator of $T$, $\tilde{T} = (2\langle\Delta\nu\rangle)^{-1}$, which is biased approximately by the same constant. According to the first-order asymptotic expression (e.g. Tassoul 1980), we can write:

$$\nu_{\ell,n} = \Delta\nu_0.\left(n + \frac{\ell}{2} + \frac{1}{4} + \alpha(\omega)\right) \text{ with } \Delta\nu_0 = \frac{1}{2T},$$

so: $\Delta\nu = \Delta\nu_0.\left(1 + \alpha(\omega+\Delta\omega) - \alpha(\omega)\right)$.

We can deduce that

$$\frac{1}{\langle\Delta\nu\rangle} \simeq \frac{1}{\Delta\nu_0}.\left(1 - \langle\alpha(\omega+\Delta\omega) - \alpha(\omega)\rangle\right)$$
$$= \frac{1}{\Delta\nu_0} - 2\pi\frac{\langle\Delta\alpha\rangle}{\Delta\omega_0} \simeq \frac{1}{\Delta\nu_0} - 2\pi\frac{{\rm d}\alpha}{{\rm d}\omega},$$

and finally $\tilde{T} \simeq T + a_\phi$.

Thus we propose to compute a quasi-non-biased estimator of $t_{\rm BCZ}$ (see results in Table 1):

$$\tilde{t}_{\rm BCZ} = \tilde{T} - \tilde{\tau}_{\rm BCZ} = \frac{1}{2\langle\Delta\nu\rangle} - \tilde{\tau}_{\rm BCZ}. \quad (6)$$

In this paper the choice is made to focus the work on the extraction of the BCZ and not to study the oscillation due to the helium ionization, although its amplitude is larger and thus easier to observe. Actually the period and the amplitude of the oscillation due to the He II ionization region can also be extracted with

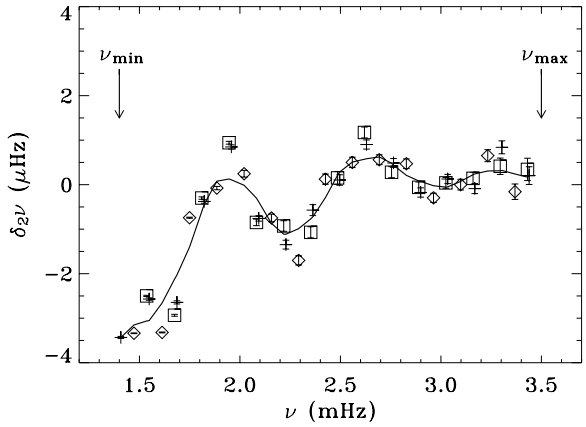


**Fig. 3.** The second difference $\delta_2\nu$ observed in the Sun with GOLF after 6-year observations. Symbols: +: $\ell = 0$, ◇: $\ell = 1$ and □: $\ell = 2$. The solid line is the smooth curve which is removed before doing the spectral analysis.

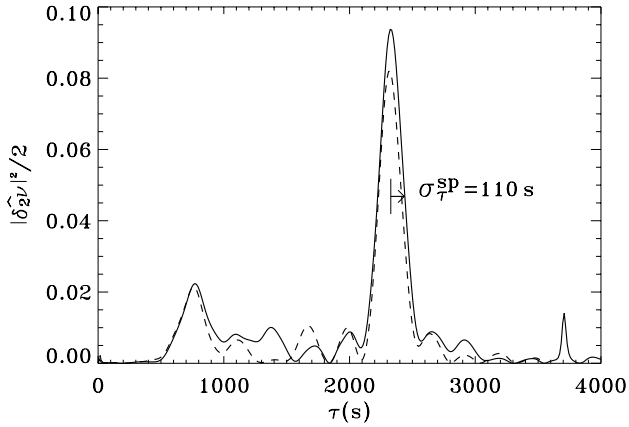


**Fig. 4.** Spectral analysis of $\delta_2\nu$ in the Sun (Fig. 3) using modes $\ell = 0, 1, 2$ (solid line) or only $\ell = 0, 1$ (dashed line). Both curves are very similar. The highest peak around 2300 s is due to the BCZ.

a spectral analysis or with a fitting as done in Fig. 2. Techniques for the helium abundance determination with asteroseismology are developed and discussed for example by Pérez Hernández & Christensen-Dalsgaard (1998), Basu et al. (2004) and Piau et al. (in preparation).

### 2.3. Example: Application to GOLF data

The previously described method is applied to the data obtained after observing the Sun over 6 years with the GOLF instrument. The second difference of low-degree modes ($\ell = 0, 1$ and 2) between 1.4 and 3.5 mHz is plotted in Fig. 3 and its analysis in Fig. 4. In this paper we denote $\widehat{X}$ the Fourier transform of $X$. The large oscillation due to the region of the He II ionization is mainly absorbed by the smooth curve but a small residue is visible around 800 s. The signature of the BCZ clearly appears around 2300 s: we have measured $\tilde{\tau}_{\rm BCZ} = 2320 \pm 110$ s and deduced $\tilde{t}_{\rm BCZ} = 1370 \pm 110$ s. These values must be compared to $t_{\rm BCZ} \simeq 1420$ s and $\tau_{\rm BCZ} \simeq 2100$ s computed with the SEISMIC$_1$ solar model from Turck-Chièze et al. (2001). As expected, the measurement of $\tilde{\tau}_{\rm BCZ}$ is biased but $\tilde{t}_{\rm BCZ}$ is correctly derived.

The extraction uncertainty – about 3% of the total acoustic radius of the star – is obtained by measuring the HWHM (half width at half maximum value) of the peak in the Fourier space. Hereafter this uncertainty is denoted $\sigma^{\rm sp}$. It depends mainly on the width of the frequency range. According to Eq. (1), the variable naturally associated with $\nu$ in the Fourier space is $2\tilde{\tau}$. Therefore the HWHM of a peak in a spectrum is typically $\sigma^{\rm sp}_{2\tilde{\tau}} \simeq \frac{1}{2(\nu_{\rm max}-\nu_{\rm min})}$. We deduce for $\tilde{t}$ that $\sigma^{\rm sp}_{\tilde{t}} = \sigma^{\rm sp}_{\tilde{\tau}} = \frac{1}{2}\sigma^{\rm sp}_{2\tilde{\tau}} \simeq \frac{1}{4(\nu_{\rm max}-\nu_{\rm min})}$. In this example, we retrieve 110 s $\sim \frac{1}{4(2.1{\rm mHz})}$. If we detect $n_0$ consecutive modes of the same degree, we can write $\sigma^{\rm sp}_{\tilde{t}} \simeq \frac{1}{4}\frac{1}{(n_0-1)\langle\Delta\nu\rangle}$, i.e.

$$\sigma^{\rm sp}_{\tilde{t}} \simeq \frac{1}{2(n_0-1)} T. \qquad (7)$$

This is why, when all the mode frequencies are well determined, using $\ell = 0, 1$ and 2 modes or only $\ell = 0$ and 1 we obtain similar results. Although they are available, we have not used $\ell = 3$ modes to be consistent with the next parts of this work: as these modes have their amplitudes reduced for geometric reasons when they are observed in disk-integrated light, the extraction of their frequencies is notably more difficult with shorter time series. With such series, only a few $\ell = 3$ modes would be measured and with a small accuracy (cf. Sect. 4.1). It is the reason why only $\ell = 0, 1$ and 2 modes have been considered.

## 3. Simulations from stellar models: The effects of the observational length

After checking the technique with long-time series, which produce excellent data quality, we have applied this method to analyze simulated observations of solar-like stars: the Sun, $\alpha$ Cen A and several other stars with different masses at different ages.

### 3.1. Stellar modelling and frequency computing

For this work, the stellar structures have been computed with the CESAM 4 stellar evolution code (Morel 1997). For the Sun, the SEISMIC$_1$ model has been used. This seismic model has been built to reproduce the sound-speed profile at best (see Couvidat et al. 2003, to find all its characteristics).

$\alpha$ Cen A is a very interesting star because it is very nearby, and it belongs to a multiple system. A set of p-mode frequencies has been measured from ground-based observations (Bouchy & Carrier 2001). This is the first time that p modes were individually identified in a solar-like star – besides the Sun, of course. These remarkable measurements give some strong and interesting constraints on its stellar structure (Thévenin et al. 2002; Thoul et al. 2003), but do not allow us to extract the BCZ with the techniques described here. The variables as $\delta_2\nu$ or $\beta^*$ (cf. Appendix A) are still too noisy after only a few days of observations (cf. Fig. 5). The spectral study of these indicators shows an oscillation corresponding to an acoustic radius of ∼1300 s which cannot be reasonably associated with a structural effect and must be considered as an artifact. The model used for this work, previously described in Ballot et al. (2003), is of a star 2.8 Gyr old, a mass of 1.16 $M_\odot$

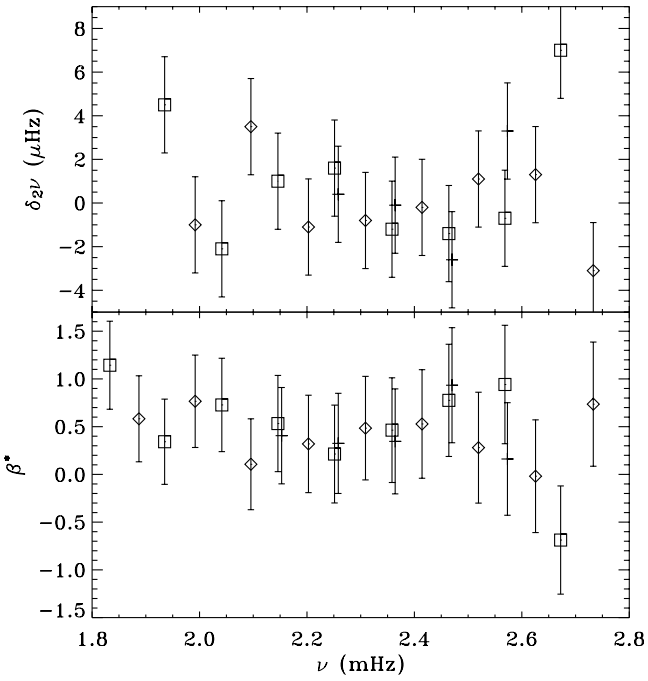


**Fig. 5.** $\delta_2\nu$ and $\beta^*$ observed in $\alpha$ Cen A (from Bouchy & Carrier 2002). Although these observations are remarkable, the accuracy obtained on the frequencies do not allow us to derive the BCZ. The resulting noise on $\delta_2\nu$ or $\beta^*$ is too large to retrieve the oscillation due to the BCZ.

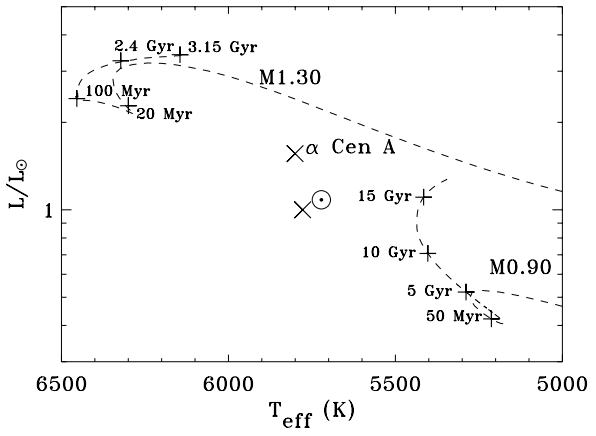


**Fig. 6.** On this HR diagram are placed the positions of models used for this study. ×: the Sun (Seismic$_1$, Turck-Chièze et al. 2001) and $\alpha$ Cen A (Ballot et al. 2003). The dashed lines are the evolutionary tracks of the models M1.30 and M0.90 (see the text for details) and + indicates some specific ages.

(Pourbaix et al. 1999), a radius of 1.24 $R_\odot$, a small convective core (0.025 $R_\odot$), a total luminosity of 1.53 $L_\odot$ and 5800 K effective temperature. This model is close to one obtained by Morel et al. (2000), but is fitted with the large and small separations observed by Bouchy & Carrier (2002). This model does not take either the recent mass estimation (1.105 ± 0.007 $M_\odot$, Pourbaix et al. 2002) or the new measurement of its radius (1.224 ± 0.003 $R_\odot$) by Kervella et al. (2003) into account. However, the modifications induced by these new constraints do not change significantly the results of this paper.

We have also built two other models of standard stars with 0.9 and 1.3 solar masses (M0.90 and M1.30 hereafter). For these models we have used the equation of state from Livermore (Rogers et al. 1996; Rogers 2000), the OPAL opacity tables (Iglesias & Rogers 1996) extended by the opacities from Alexander & Ferguson (1994) and the nuclear reaction rates from Adelberger et al. (1998). The atmospheres have been rebuilt according to the classic Hopf law (e.g. Mihalas 1970). The convective energy transport has been processed with the standard Mixing Length Theory (Böhm-Vitense 1958) using a mixing length parameter $\alpha = 1.7$. No overshoot has been introduced. The microscopic diffusion has also been treated according to the formalism from Michaud & Proffitt (1993) to take into account the gravitational settling of helium and heavier elements. The initial helium abundance was $Y_i = 0.270$ and the initial metallicity $(Z/X)_i = 0.0289$. Structures of M0.90 and M1.30 have been computed at several ages. Table 1 gives $T$ and $t_{\rm BCZ}$ for all these stars and Fig. 6 shows their positions in a HR diagram.

From the structures of these stars, the eigenfrequencies of low-degree ($\ell = 0, 1$ and 2) acoustic modes have been computed with the Aarhus adiabatic pulsation package (Christensen-Dalsgaard 1982, 1998).

### 3.2. Reference cases: Long observations

For each model, we have selected the low-degree modes $\ell = 0, 1$ and 2 whose orders were contained between $n = 14$ and 26. This selection is an example of the frequency set we shall be able to reach with the future asteroseismic missions. We have discussed in Ballot et al. (2003) the influence of the available range of frequencies. It is clear from Fig. 2 that the low-frequency range is extremely useful for the extraction of the BCZ. The choice of the frequency range we have made here is reasonable: it is based on the existing observations of the Sun or $\alpha$ Cen A. It is crudely extended to the other modelled stars: the aim of this paper is not to discuss the amplitude or the excitation of the modes (about this subject, see for example Houdek et al. 1999; Samadi et al. 2003). From this selected frequency set, $\delta_2\nu$ is computed and $\tilde{t}_{\rm BCZ}$ extracted with the method described previously. The results are given in Table 1. We remark that the uncertainties – measured as the HWHM of the peak – are always around 4–5%, which is consistent with Eq. (7). However, we note that the error is always significantly smaller than this uncertainty: it is smaller than 1.5%, and generally than 1%. We can also note that the result is quasi-non-biased, nevertheless it seems that $t_{\rm BCZ}$ is systematically slightly underestimated. We have also fitted expression (5) using the outputs of the spectral analysis as guessing parameters. Thus a new estimation of $\tilde{t}_{\rm BCZ}$ is obtained with a new uncertainty $\sigma_{\tilde{t}}^{\rm fit}$ provided by the least-squares fitting method itself (results in Table 1). This shows that this method is more accurate than the previous one, in the sense that the error bar $\sigma_{\tilde{t}}^{\rm fit}$ is strongly reduced (1–2%) in comparison to $\sigma_{\tilde{t}}^{\rm sp}$. This error bar is consistent with the real error made. However the value of $t_{\rm BCZ}$ itself is not improved. With these reference analyses we can also estimate $\sigma_t^{\rm met}$, the intrinsic error of the method, at about 1.5%.

This error mainly includes the effects of the limited number of points and the unknown residual bias of the estimator.

After computing this reference, noise has been added to the frequencies to simulate the effect of the observational interval.

### 3.3. Principle of the noise simulations

All the simulations of this part are based on the same principle. Noise has been randomly added to a given frequency set. We have assumed that this noise follows a Gaussian probability distribution with a standard deviation $\sigma_\nu = 1/T_{\rm obs}$, where $T_{\rm obs}$ is the simulated observational duration. This assumption is a little rough: the error depends also on the width and the amplitude of the mode, i.e. on the energy and the damping of the mode. Nevertheless this law gives the global behaviour because it is the error due to the spectral resolution reached which effectively dominates the solar-like stars.

We have computed 10 000 Monte Carlo realizations by processing 10 000 noise-frequency sets and analyzing them. Eight different observational lengths have been simulated: $T_{\rm obs}$ = 15, 30, 60, 90, 120, 150, 300 and 540 days. The analysis consists of the study of the Fourier domain of $\delta_2\nu$ (cf. Sect. 2.2) and other similar variables (Sect. 2.1). The peak corresponding to the BCZ has been *automatically* looked for to determine $\tilde{\tau}_{\rm BCZ}$, $\tilde{T}$ has been computed and $\tilde{t}_{\rm BCZ}$ extracted.

### 3.4. Comparison of different variables

The aim of this first set of simulations is to validate the choice of $\delta_2\nu$ as a good tracer of the BCZ and to determine a minimal observational length to correctly derive the BCZ. Taking the solar case, we have realized the simulations described in Sect. 3.3. We have used different variables as tracers of the BCZ: $\delta_2\nu$ of course, $\Delta\nu$, $\delta_4\nu$, $\delta_6\nu$ and finally $\beta^*$ (cf. Appendix A). For each simulated observational duration and for each studied variable, we have counted how many times out of the 10 000 realizations the acoustic radius of BCZ has been correctly determined within 5% ($\simeq \sigma_{\tilde{t}}^{\rm sp}$, cf. Sect. 3.2) in comparison with the radius obtained with a non-noisy frequency table. The results (Fig. 7) confirm the choice done in Sect. 2.1: among the different differences $\delta_k\nu$, the best results are obtained using $\delta_2\nu$. The results obtained with $\beta^*$ and $\Delta\nu$ are almost the same. The small difference comes from failures of the automatic peak search which is disturbed by other strong peaks (see Appendix B).

Figure 8 shows the spectral analyses of $\delta_2\nu$ for some realizations and for the different observational lengths. These pictures clearly indicate that the BCZ signature appears more and more frequently with the increase of the observational duration. These simulations show that 15 and 30 days are not sufficiently long to derive the BCZ position with this technique for a star like the Sun. But after 90 days, $\delta_2\nu$ allows us to retrieve the correct position two times out of three; in the other cases the BCZ is not determined or derived with a bad location. Finally after 150 days, we can correctly determine it for 90% of the simulated observations.

Figure 9 shows the distribution of the extracted $\tilde{t}_{\rm BCZ}$ for three simulations $T_{\rm obs}$ = 90, 150 and 300 days. This

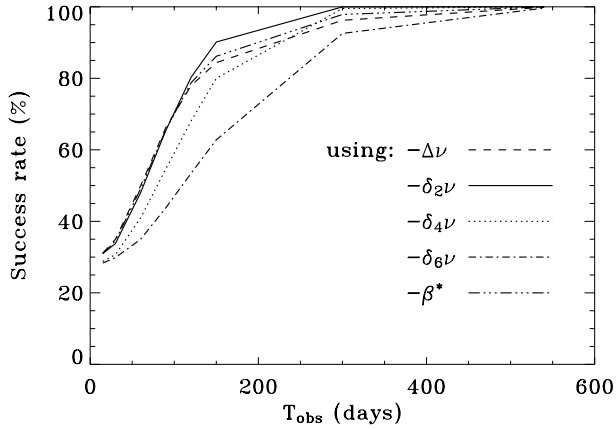


**Fig. 7.** Effect of the observational length ($T_{\rm obs}$) on the determination of the BCZ in the solar case (cf. simulations described in Sect. 3.4). Each line corresponds to the use of a different variable. For each one, the rate of good determination of the BCZ acoustic radius (within 5%) is plotted as a function of $T_{\rm obs}$. The best results are obtained with $\delta_2\nu$: with a 150-day observation the success rate is around 90%.

figure illustrates two distinct phenomena. Firstly the number of false detections increases with shorter time series: the spectrum of $\delta_2\nu$ is noisier and an artifact can be detected instead of the real peak. Some recurrent artifacts, as the one observed around 1850 s, are due to the quasi-periodic spacing of the points. Secondly the distribution is broader with a shorter observational length. We can measure this dispersion ($\sigma_{\tilde{t}}^{\rm obs}$) to estimate the supplementary noise introduced by the limited observational time. Table 2 shows $\sigma_{\tilde{t}}^{\rm obs}$ obtained for the different simulations. It appears that for 150 days $\sigma_{\tilde{t}}^{\rm obs} \simeq 1.6\%$. In consequence, 150 days seems to be a good compromise to observe a star like the Sun and to hope to extract the BCZ.

### 3.5. Effect of the stellar structure

However the amplitude of the BCZ signature depends on the structure of the observed star. It depends on $t_{\rm BCZ}/T$ (cf. Eq. (4)) and on the physical conditions of the transition. Effectively in a not very stratified young star, the step of the sound-speed second derivative at the BCZ is smaller than in a more evolved star. For example, in the case of M1.30: at 20 Myr, $\left[\frac{{\rm d}^2c^2}{{\rm d}r^2}\right]_{\rm BCZ^-}^{\rm BCZ^+} \simeq 5\times10^{-6}$ s$^{-2}$ and $\simeq 5\times10^{-5}$ s$^{-2}$ at 3.15 Gyr. It is the reason why the signatures of the BCZ in $\delta_2\nu$ are so different in the two cases (Figs. 10 and 11). It is important to notice that the magnification coefficients $(2\sin(\pi\frac{t_{\rm BCZ}}{T}))^2$ are nearly the same at these two ages (3.9 at 20 Myr, 4.0 at 3.15 Gyr from Table 1). This strong variation of $\frac{{\rm d}^2c^2}{{\rm d}r^2}$ is due to the strong composition gradient which appears beneath the convective zone mainly because of the settling of the helium and heavy elements. If the microscopic diffusion is not taken into account, this effect totally disappears. Thus the study of the signature amplitude could give information on the efficiency of diffusion phenomena.

We have done the same kind of Monte Carlo simulations as previously for the different modelled solar-like stars. $\delta_2\nu$ is used as a BCZ tracer, except for M0.90 at 15 Gyr where $\beta^*$ is used. Since $t_{\rm BCZ}/T = 0.32$ for this model, the signature of BCZ

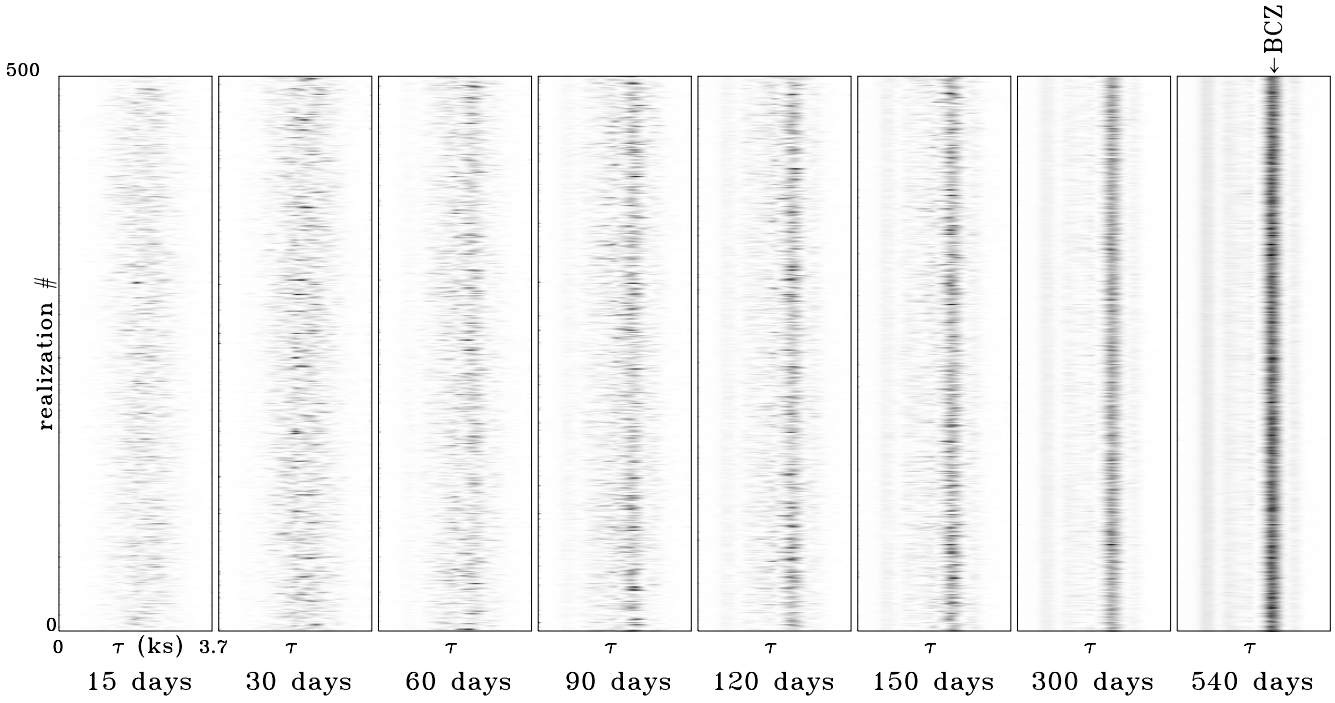


**Fig. 8.** Effect of the observational length ($T_{\rm obs}$) on the determination of the BCZ in the solar case (cf. simulations described in Sect. 3.4). Each picture shows the spectral analyses of $\delta_2\nu$ in 500 realizations for the different simulated observational lengths. In each picture, each line corresponds to a spectrum similar to the one plotted in Fig. 4.

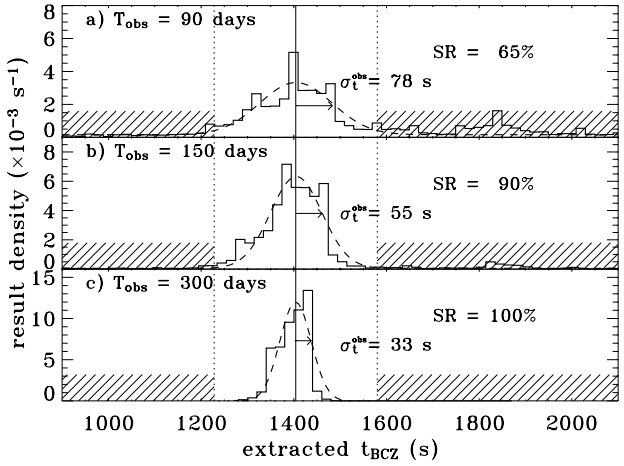


**Fig. 9.** Distributions of results of $\tilde{t}_{\rm BCZ}$ extraction with $\delta_2\nu$ in the solar case for 3 observational lengths ($T_{\rm obs}$ = 90, 150 and 300 days). The hatched areas indicate the detections considered as bad (i.e. with an error larger than 5%, see the text and Fig. 7). For each simulation, the success rate (SR), i.e. the rate of good detections, is given. The dashed line is a normal distribution with a standard deviation $\sigma_{\tilde{t}}^{\rm obs}$ fitting the result distribution. The $Y$ axis represents a "density of results": for each bin $[t, t + {\rm d}t]$, the number of realizations where $\tilde{t} \in [t, t + {\rm d}t]$ is divided by the total number of realizations and normalized by the bin size (d$t$). Thus the integral of this quantity is always equal to one.

is not magnified in $\delta_2\nu$ (cf. Fig. 1) and then $\beta^*$ is a better indicator. The results (Fig. 12) show interesting disparities in the different stars. Especially, for M1.30 at 3.15 Gyr the success rate reaches 90% after only two months. We also notice that $\alpha$ Cen A has the same behaviour than the Sun. After a 150-day observation the success rate is greater than 75% for all the modelled stars.

**Table 2.** For each simulated observational length ($T_{\rm obs}$) one indicates the frequency error bars used ($\sigma_\nu$), the success rate of $\tilde{t}_{\rm BCZ}$ extraction (SR) and the dispersion of good extractions $\sigma_{\tilde{t}}^{\rm obs}/T$.

| $T_{\rm obs}$ (days) | $\sigma_\nu$ (nHz) | SR | $\sigma_{\tilde{t}}^{\rm obs}/T$ |
|---|---|---|---|
| 60 | 193. | 48.0% | 3.16% |
| 90 | 129. | 65.4% | 2.22% |
| 120 | 96. | 80.3% | 1.85% |
| 150 | 77. | 90.2% | 1.58% |
| 300 | 39. | 100.0% | 0.96% |
| 540 | 21. | 100.0% | 0.49% |

In conclusion it appears that, for some stars, two or three months are enough to correctly derive the BCZ. Nevertheless, to determine it in a majority of solar-like stars, 150 days (which corresponds in the simulations to an error $\sigma_\nu$ = 0.08 $\mu$Hz) seems to be a good observational length. However these simulations have some limitations: the main one is to have not fully taken into account all the effects of the stochastic excitation, especially the dependence of the error upon the frequency. To make a realistic study of this effect, we have used real data.

## 4. Real data: VIRGO data analysis

To simulate as realistically as possible the future asteroseismic missions, we have used photometric data provided by the

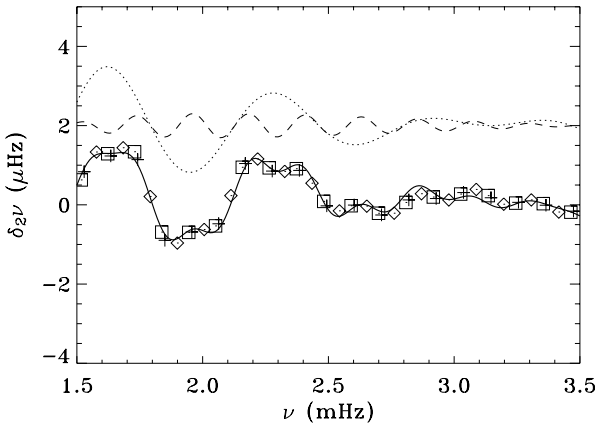


**Fig. 10.** $\delta_2\nu$ for M1.30 at 20 Myr. See Fig. 2 for the description. For this not very stratified young star, the amplitude of the BCZ signature is around 0.1−0.3 $\mu$Hz.

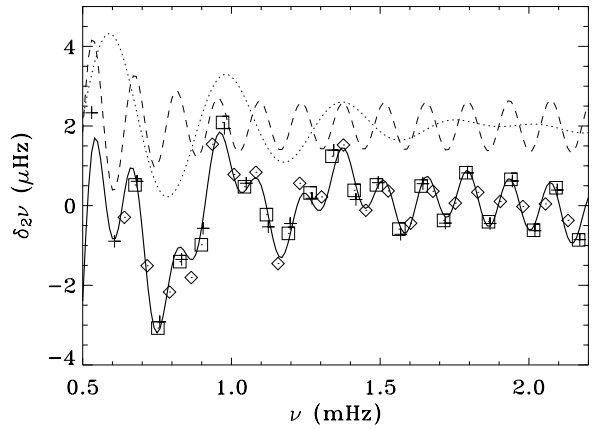


**Fig. 11.** $\delta_2\nu$ for M1.30 at 3.15 Gyr. See Fig. 2 for the description. For this relatively old star, the amplitude of the BCZ signature is around 0.7–1 $\mu$Hz.

Sun Photometers (SPM) of the VIRGO[3] instrument (Fröhlich et al. 1997) aboard the SoHO mission. The VIRGO/SPM measures the solar irradiance at a 60-second cadence through 5-nm wide filters centred at blue (402 nm), green (500 nm) and red (862 nm) wavelengths calibrated following Jiménez et al. (1999). Here we have summed the three channels to have a good proxy of a white solar irradiance. Series of 2240 days have been used starting on February 13 1996, at the minimum of activity cycle 22/23, up to the maximum of solar activity cycle 23. This data set has been cut in subseries of 150 continuous days. To avoid a significant reduction on the duty cycle of some of the series, we have not taken into account the second half of 1998 where two extended gaps in coverage are present due to the loss and recovery procedure of the SoHO mission. Thus, 12 subseries of more than 95% duty cycle have been retained for the current analysis.

### 4.1. Determination of frequencies

Once the time series have been extracted and the power spectrum computed, a maximum likelihood fitting code (e.g.

[3] Variability of Solar IRradiance and Gravity Oscillations.

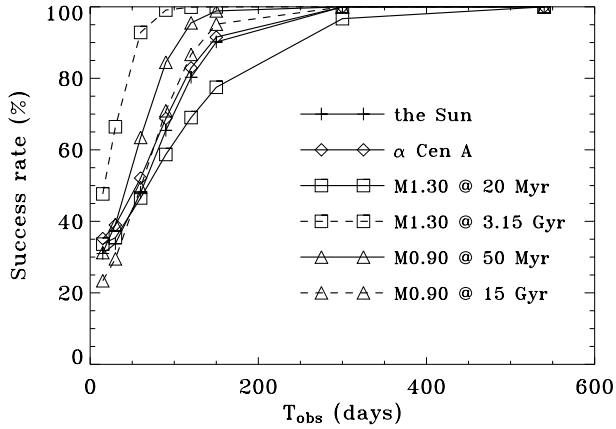


**Fig. 12.** Effect of the observational length ($T_{\rm obs}$) on the determination of the BCZ for different modelled stars (cf. Table 1 and the simulations described in Sect. 3.5). The different symbols correspond to the different stars, and for the same star, different lines indicate different ages. For each one, the rate of good determination of the BCZ acoustic radius (within 5%) derived from $\delta_2\nu$ – except for M0.90@15Gyr: $\beta^*$ – is plotted as a function of $T_{\rm obs}$.

Appourchaux et al. 1998) has been used to deduce the parameters of the solar resonances. Because of their proximity in frequency and the relatively low frequency resolution of our series, we have fitted together the modes $\ell = 0$ and 2 and the modes $\ell = 1$ and 3. We have used symmetric and asymmetric Lorentzian profiles to describe each resonance. However, no systematic differences have been observed in the results and the symmetric ones have been favoured. In this paper our main interest is the extracted central frequency of the modes. To obtain the best stability on the fittings we have fixed the amplitude ratio of the components in a multiplet and the splittings. These values are well known for the solar case and should be known for the future observation of other stars. We are developing some new techniques that will provide the angle between the rotation axis of the star and the line of sight (which fixes the amplitude ratio of the mode components) and their splitting (Ballot et al. in preparation).

### 4.2. BCZ extraction

We have analyzed the second difference obtained in the twelve series to extract the BCZ. The analysis is done with $\ell = 0, 1$ and 2 modes or only with $\ell = 0$ and 1. We have used the modes whose frequency is between 2.10 and 3.51 mHz. These modes are unambiguously detected. The typical error bars $\sigma_\nu$ depend on the frequency and they typically vary in the range 0.07−0.25 $\mu$Hz. The minimum error is for the frequencies around 3 mHz, where the mode amplitudes are the largest. Although some $\ell = 3$ modes are measured, they have not been considered for the analyses because their error bars are typically twice as large as those of the other extracted modes.

Figure 13 shows results for three typical examples of the considered series. In the case a), the detection is bad and no peak can indicate the BCZ; in b), a peak is visible at the right place, but an artifact with a larger amplitude prevents us from

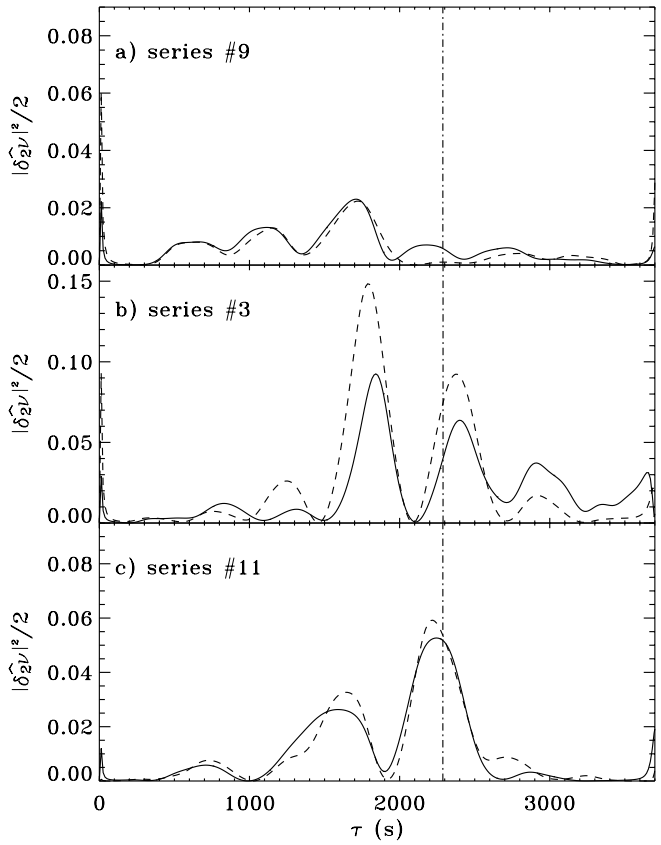


**Fig. 13.** Spectral analysis of $\delta_2\nu$ for three VIRGO series, using $\ell = 0, 1$ and 2 modes (solid curve) and only $\ell = 0$ and 1 (dashed curve). The dot-dashed line indicates the expected BCZ position.

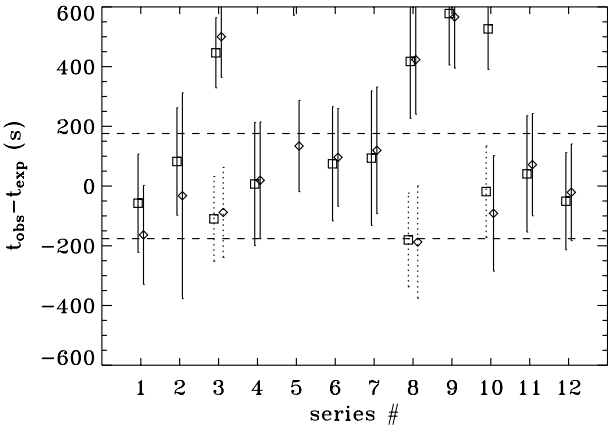


**Fig. 14.** Detected acoustic radius of the BCZ compared to its expected value for the 12 continuous series. The symbols with solid error bars indicate the results of detection. □: $\ell = 0, 1, 2$ modes are used; ◇: $\ell = 0, 1$ only. The dashed lines indicate the zone where $|\tilde{t}_{\mathrm{BCZ(obs.)}} - t_{\mathrm{BCZ(exp.)}}| < 5\%\ T$. For the bad detections the position of the peak which have the second larger amplitude is also plotted with a dotted error bar.

detecting it without ambiguity; the last case c) is an example of a good detection.

In Fig. 14 the summary of all series is shown. It appears that the results are better when only the modes $\ell = 0$ and 1 are taken into account: 9 detections out of 12 are correct instead of 7 if the $\ell = 2$ modes are also used. The detection fails due to an artifact in two series (# 3 and # 10). Effectively the peak with the second larger amplitude contains the information about the BCZ. With two series (# 8 and # 9) no correct signature can be extracted. The success rate seems to be slightly worse than in the previous simulations (75% instead of 90%, Sect. 3.4). This can be explained by the underestimation of the error bars for several modes made in the previous simulations. However this success rate is just indicative, as the statistical sample is very small. Thus the loss of quality in term of "success rate" is real and notable but cannot be accurately quantified with this analysis.

## 5. Large windowing effect

The last part of this work consists of studying the effects of long data gaps (∼5−12 months) during seismic observations. This could influence the observational strategy in future missions where time is shared between exoplanet finding and asteroseismology. The possibility of observing the same field again after an interruption must be considered.

### 5.1. Simulations: Influence on the frequency determination

As has been seen previously, the critical point for a good extraction is the accurate determination of the eigenfrequencies. Thus, we have studied how the large windowing influences this determination. We have built an ideal power spectrum $L_{\mathrm{mod}}(\nu)$ containing $\ell = 0$ and 1 modes modelled with different widths and corresponding to an observation of a few years. From this a noisy amplitude $A(\nu)$ spectrum has been computed using

$$A(\nu) = (g_1(\nu) + \mathrm{i}\, g_2(\nu)) \cdot \sqrt{\frac{L_{\mathrm{mod}}(\nu)}{2}} \tag{8}$$

where $g_1$ and $g_2$ are two random functions following a normal distribution with a null mean value and a standard deviation equal to one (Fierry Fraillon et al. 1998). We have then computed the associated time series. In these time series, five non-continuous 30-day long subseries have been randomly chosen and analyzed as a continuous 150-day long observation: we have computed the corresponding power spectrum and fitted the modes to extract the frequencies. 10 000 similar Monte Carlo realizations have been made. For each one the fitted frequencies have been compared to the input frequencies to obtain the dispersion of the frequencies around the input one. We have also made Monte Carlo simulations with continuous 150-day simulated observations, containing the same modes as in the previous simulations. The frequencies have been extracted and compared to the input ones to obtain the reference dispersions.

For each simulated mode, the frequency dispersion obtained in both cases (continuous series or not) are compared (see Ballot et al. 2004). It appears that the frequency determination is degraded by the windowing (i.e. the dispersion is broader than in the reference case) only if the peak is narrower than one or two spectrum bins. For a 150-day observation, the spectrum bin is 77 nHz. As in the VIRGO series the widths of

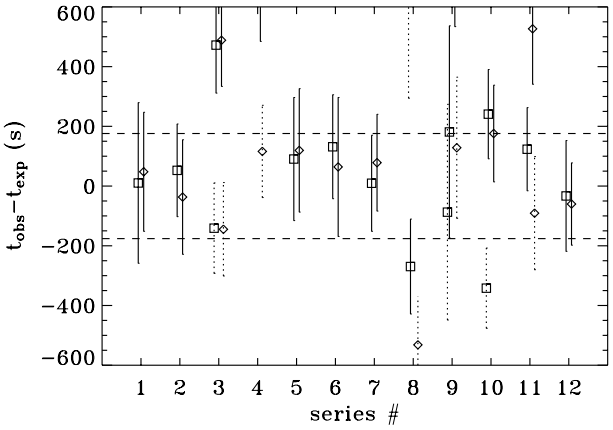


**Fig. 15.** Similar to Fig. 14 for the discontinuous series.

the modes we can reach are broader than 150 nHz, the windowing does not seem to have strong effects on the frequency determination and, as a consequence, on the stellar structure analysis.

### 5.2. Real data: Effect of the stellar activity

A similar work can be done with the VIRGO data. We can attempt to retrieve the BCZ with the frequencies extracted from twelve non-continuous series of VIRGO data, with five months of observations randomly distributed over five years. We have used the same methods as those described in Sect. 4.

Figure 15 shows the results of the extraction and can be compared to Fig. 14. Seven series – instead of nine series in Sect. 4.2 – out of twelve are correct. This rate does not change if $\ell = 2$ modes are also considered. These results seem slightly degraded, whereas the simulation had not forecast it. However this difference is not statistically relevant in view of the small size of the sample. Nevertheless the dispersion is a little greater than in Fig. 14. This possible degradation can be due to the activity of the Sun. Each series contains data taken during the maximum and the minimum because of the cuttings. When the activity changes, the frequencies of the modes change too, especially at high frequencies (see Jiménez-Reyes et al. 2003a,b). The variation can reach a few micro-hertz. In these non-continuous series, the frequencies change between each 1-month run. The measured frequencies are mixings of all these, a supplementary noise is added to the frequency measurement for such data series.

## 6. Discussion

The method developed and used for this work to extract the BCZ is robust, fast and easy to set up without any a priori assumption, especially, no input model structure is needed. This is why the given results are the *acoustic* radii and not distances.

This technique can be very interesting to apply to a large set of stellar seismic observations. It will not be possible to use fine techniques on all future observed stars and such a method could, for example, provide information on a statistical sample of stars, like an open cluster. Moreover, after this study, it clearly appears that the mode excitation must be taken into account to check the different analysis methods. In this case, one month is a too short observational length to extract the signature of the BCZ from frequencies. Although two months can be sufficient for more massive evolved solar-like stars, a good compromise requires us to observe at least 150 days to get information from a large sample of solar-like stars. These observations can be fragmented in some runs that are spread on several years, but the effects of the stellar activity must be properly studied. It will be especially useful to follow the activity of the stars and try to correct its effect on the frequencies. Thus we could improve the frequency determination and so our knowledge of the stellar internal structure. The present studies on the effects of solar activity on the acoustic mode characteristics (e.g. Jiménez-Reyes et al. 2004) will be extremely useful to progress on this point.

*Acknowledgements.* We want to thank the CNES institution and the GOLF and VIRGO teams for the skill and dedication of the many engineers and scientists in Europe and USA. SoHO is an international collaboration programme of the European Space Agency and the National Aeronautics Space Administration.

## Appendix A: $\beta^*$ computing

To compute $\beta^*$, the expression described by Roxburgh & Vorontsov (2001, Eq. (37)) is applied:

$$\beta^* \simeq \frac{1}{2}\frac{\nu_{\ell,n+1}+\nu_{\ell,n}}{\nu_{\ell,n+1}-\nu_{\ell,n}} - \left(n - \frac{\ell}{2} + \frac{3}{2}\right) + \frac{\ell(\ell+1)}{\pi}a$$

where $a$ is obtained by fitting $D_\delta(\omega)$ with a linear form:

$$D_\delta(\omega) \simeq a + b\omega.$$

$D_\delta(\omega)$ is defined from the small separation and computed with the next expression:

$$D_\delta(\omega) \simeq \frac{\pi}{2}\frac{\nu_{\ell,n} - \nu_{\ell+2,n-1}}{(2\ell+3)\Delta\nu}$$

where $\Delta\nu$ is the large separation.

## References

Adelberger, E. G., Austin, S. M., Bahcall, J. N., et al. 1998, Rev. Mod. Phys., 70, 1265
Alexander, D. R., & Ferguson, J. W. 1994, ApJ, 437, 879
Appourchaux, T., Gizon, L., & Rabello-Soares, M.-C. 1998, A&AS, 132, 107
Böhm-Vitense, E. 1958, Z. Astrophys., 46, 108
Baglin, A., & The CoRoT Team 1998, in New Eyes to See Inside the Sun and Stars, IAU Symp., 185, 301
Ballot, J., Turck-Chièze, S., García, R. A., & Nghiem, P. 2003, in Asteroseismology Across the HR Diagram, ed. M. Thompson, M. Cunha, & M. Monteiro, P497
Ballot, J., García, R. A., & Turck-Chièze, S. 2004, in Stellar Structure and Habitable Planet Finding, ed. F. Favata, & S. Aigrain, ESA SP-538: 2nd Eddington workshop, 265
Basu, S. 1997, MNRAS, 288, 572
Basu, S., Mazumdar, A., Antia, H. M., & Demarque, P. 2004, MNRAS, 350, 277
Bouchy, F., & Carrier, F. 2001, A&A, 374, L5
Bouchy, F., & Carrier, F. 2002, A&A, 390, 205

Brun, A. S., Turck-Chièze, S., & Zahn, J. P. 1999, ApJ, 525, 1032
Christensen-Dalsgaard, J. 1982, MNRAS, 199, 735
Christensen-Dalsgaard, J. 1998, Lecture Notes on Stellar Oscillations, http://astro.ifa.au.dk/~jcd/oscilnotes/
Christensen-Dalsgaard, J., Gough, D. O., & Thompson, M. J. 1991, ApJ, 378, 413
Christensen-Dalsgaard, J., Monteiro, M. J. P. F. G., & Thompson, M. J. 1995, MNRAS, 276, 283
Couvidat, S., Turck-Chièze, S., & Kosovichev, A. G. 2003, ApJ, 599, 1434
Favata, F., Gimenez, A., & Eddington Science Team 2003, Solar and Solar-Like Oscillations: Insights and Challenges for the Sun and Stars, 25th Meet. IAU, Joint Discussion 12, 18 July, Sydney, Australia, 12
Fierry Fraillon, D., Gelly, B., Schmider, F. X., et al. 1998, A&A, 333, 362
Fröhlich, C., Andersen, B., Appourchaux, T., et al. 1997, Sol. Phys., 170, 1
Gough, D. O. 1990, in Progress of Seismology of the Sun and Stars, LNP, 367, 283
Houdek, G., Balmforth, N. J., Christensen-Dalsgaard, J., & Gough, D. O. 1999, A&A, 351, 582
Iglesias, C. A., & Rogers, F. J. 1996, ApJ, 464, 943
Jiménez, A., Roca Cortés, T., Severino, G., & Marmolino, C. 1999, ApJ, 525, 1042
Jiménez-Reyes, S. J., García, R. A., Jiménez, A., & Chaplin, W. J. 2003a, ApJ, 595, 446
Jiménez-Reyes, S. J., Jiménez, A., & García, R. A. 2003b, in Local and Global Helioseismology: the Present and Future, ESA SP-517: GONG+ 2002, 321
Jiménez-Reyes, S. J., Chaplin, W. J., Elsworth, Y., & García, R. A. 2004, ApJ, 604, 969
Kervella, P., Thévenin, F., Ségransan, D., et al. 2003, A&A, 404, 1087
Lopes, I., & Turck-Chièze, S. 1994, A&A, 290, 845
Lopes, I., Turck-Chièze, S., Michel, E., & Goupil, M. 1997, ApJ, 480, 794
Marchenkov, K., Roxburgh, I., & Vorontsov, S. 2000, MNRAS, 312, 39
Mazumdar, A., & Antia, H. M. 2001, A&A, 368, L8
Michaud, G., & Proffitt, C. R. 1993, in Inside the Stars, ASP Conf. Ser., 40, IAU Coll., 137, 246
Mihalas, D. 1970, Stellar atmospheres, Series of Books in Astronomy and Astrophysics (San Francisco: Freeman)
Monteiro, M. J. P. F. G., Christensen-Dalsgaard, J., & Thompson, M. J. 1994, A&A, 283, 247
Monteiro, M. J. P. F. G., Christensen-Dalsgaard, J., & Thompson, M. J. 2000, MNRAS, 316, 165
Morel, P. 1997, A&AS, 124, 597
Morel, P., Provost, J., Lebreton, Y., Thévenin, F., & Berthomieu, G. 2000, A&A, 363, 675
Pérez Hernández, F., & Christensen-Dalsgaard, J. 1998, MNRAS, 295, 344
Piau, L., & Turck-Chièze, S. 2002, ApJ, 566, 419
Pourbaix, D., Neuforge-Verheecke, C., & Noels, A. 1999, A&A, 344, 172
Pourbaix, D., Nidever, D., McCarthy, C., et al. 2002, A&A, 386, 280
Rogers, F. J. 2000, Phys. of Plasmas, 7, 51
Rogers, F. J., Swenson, F. J., & Iglesias, C. A. 1996, ApJ, 456, 902
Roxburgh, I. W., & Vorontsov, S. V. 1994, MNRAS, 268, 880
Roxburgh, I. W., & Vorontsov, S. V. 1996, MNRAS, 278, 940
Roxburgh, I. W., & Vorontsov, S. V. 2001, MNRAS, 322, 85
Roxburgh, I. W., & Vorontsov, S. V. 2003, Ap&SS, 284, 187
Samadi, R., Nordlund, Å., Stein, R. F., Goupil, M. J., & Roxburgh, I. 2003, A&A, 403, 303
Spiegel, E. A., & Zahn, J.-P. 1992, A&A, 265, 106
Tassoul, M. 1980, ApJS, 43, 469
Thévenin, F., Provost, J., Morel, P., et al. 2002, A&A, 392, L9
Thoul, A., Scuflaire, R., Noels, A., et al. 2003, A&A, 402, 293
Turck-Chièze, S., Couvidat, S., Kosovichev, A. G., et al. 2001, ApJ, 555, L69
Ventura, P., Zeppieri, A., Mazzitelli, I., & D'Antona, F. 1998, A&A, 331, 1011
Vorontsov, S. V., Baturin, V. A., & Pamiatnykh, A. A. 1991, Nature, 349, 49

# Online Material

## Appendix B: Simulation examples

This appendix gives two different realizations among the 10 000 simulations described in Sect. 3.4. The simulated observations are 150 days long. In both realizations the variables and their spectral analyses are plotted. Figure B.1 presents an example where the determination is very good for all variables. In the case shown in Fig. B.2, the detection fails with several variables. This detection failure is due to the presence of high peaks which misleads the automatic search for the maximum.

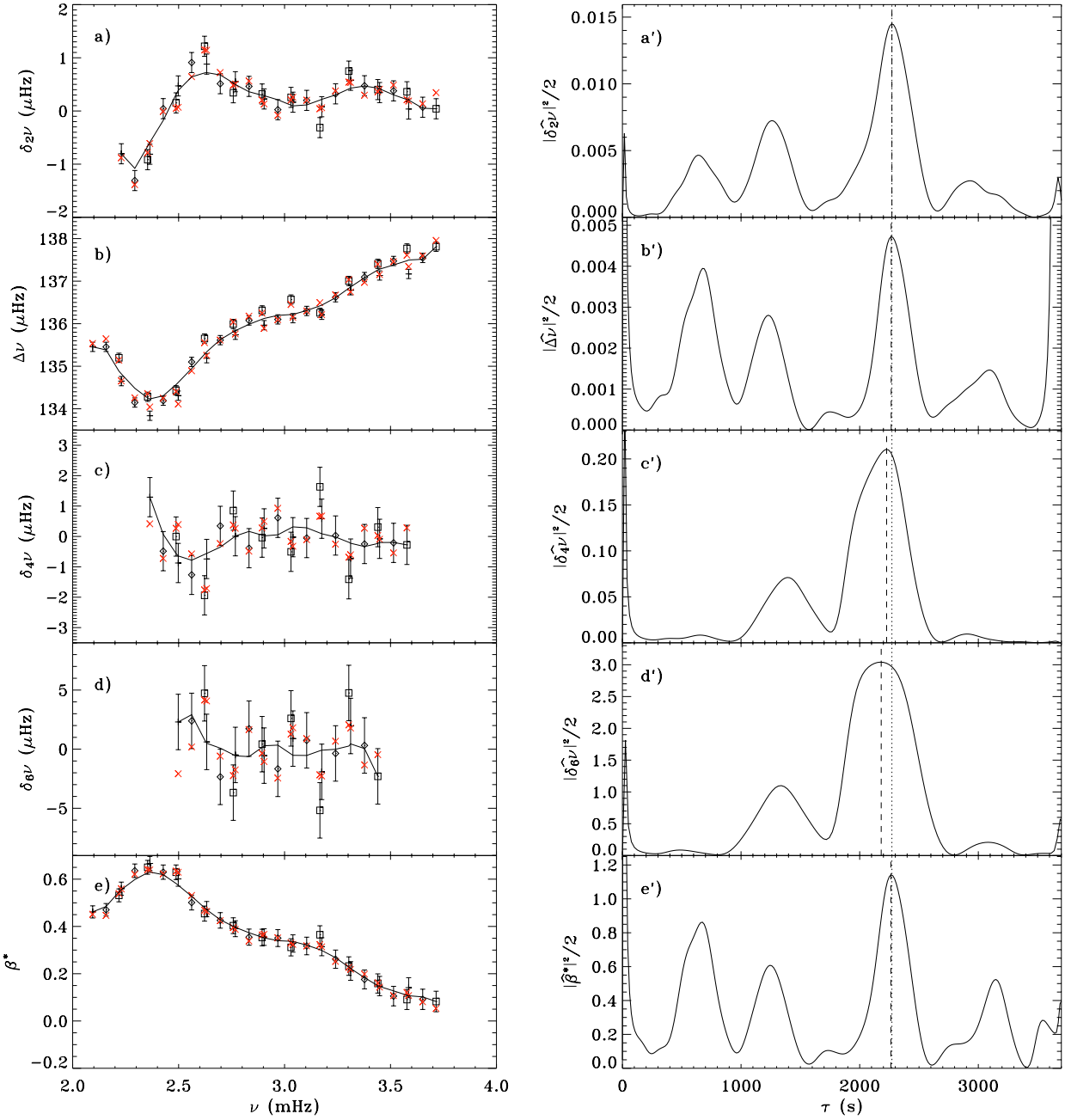


**Fig. B.1.** An example of one realization coming from the Monte Carlo simulation for a 150-day simulated observation (cf. Sect. 3.4). **a)–e)** The variables $\Delta\nu$, $\delta_2\nu$, $\delta_4\nu$, $\delta_6\nu$ and $\beta^*$. Symbols with error bars: +: $\ell = 0$, ◇: $\ell = 1$ and □: $\ell = 2$. The crosses (×) indicate the theoretic values (without noise). **a′)–e′)** The spectral analyses of these variables. The dotted line shows the expected position for the BCZ peak, the dashed line gives the extracted position.

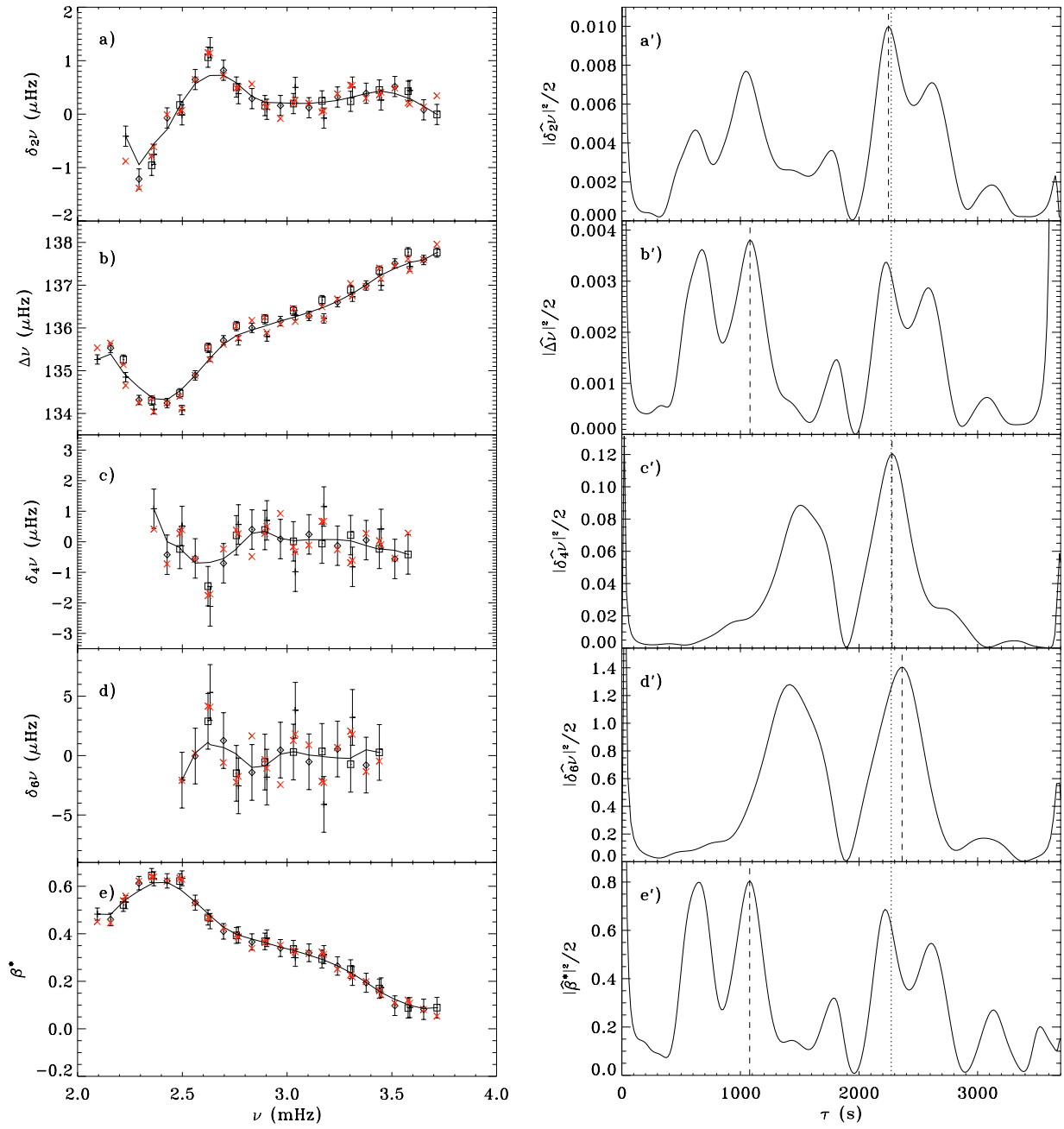


**Fig. B.2.** An example of one realization coming from the Monte Carlo simulation for a 150-day simulated observation (cf. Sect. 3.4). **a)–e)** The variables $\Delta\nu$, $\delta_2\nu$, $\delta_4\nu$, $\delta_6\nu$ and $\beta^*$. Symbols with error bars: +: $\ell = 0$, ◇: $\ell = 1$ and □: $\ell = 2$. The crosses (×) indicate the theoretic values (without noise). **a′)–e′)** The spectral analyses of these variables. The dotted line shows the expected position for the BCZ peak, the dashed line gives the extracted position.